

# Interferometric $^{12}\text{CO}$ Observations of the Central Disk of NGC 4631: An Energetic Molecular Outflow

Richard J. Rand

Dept. of Physics and Astronomy, University of New Mexico, 800 Yale Blvd, NE, Albuquerque, NM 87131

## ABSTRACT

We present interferometric observations of CO  $J = 1 - 0$  emission in the central regions of the edge-on galaxy NGC 4631, known for its extended gaseous halo and its tidal interactions. Previous single-dish observations revealed that almost all of the CO emission arises from a central ring or bar-like structure of length  $\sim 4$  kpc. We confirm this structure at higher resolution, and find that it is bent at the center, reflecting the overall bend in this galaxy apparent from optical images. The kinematic evidence favors a rigidly rotating ring over a bar. The gaseous halo emission in several tracers is concentrated above and below this molecular structure. To the north of an emission peak at the eastern end of the structure is an extraplanar feature showing filamentary and shell-like properties which we interpret as an energetic molecular outflow. The energies involved are difficult to estimate, but are probably of order  $10^{54}$  ergs or more. The CO concentration in the disk below this structure coincides with a bright HII region complex, a peak of radio emission, and the brightest X-ray feature in the inner disk of the galaxy seen in a ROSAT HRI map, all suggesting intense star formation. A filament of radio continuum emission may also have a footprint in this region of the disk. The origin of the outflow is unclear.

*Subject headings:* galaxies: individual (NGC 4631): — galaxies: interstellar matter — galaxies: evolution — radio lines: galaxies — interstellar: molecules

## 1. Introduction

NGC 4631 is one of the best examples of a nearby edge-on galaxy with a star formation driven outflow resulting in a bright and extended gaseous halo. This is seen in many tracers: H $\alpha$  (Rand, Kulkarni, & Hester 1992; Hoopes, Walterbos, & Rand 1999), radio continuum (e.g. Ekers & Sancisi 1977; Hummel & Dettmar 1990; Golla & Hummel 1994), and X-rays (Wang et al. 1995; Vogler & Pietsch 1996). This galaxy is undergoing interactions with two companions, NGC 4627 and NGC 4656, and shows a complex pattern of tidal features seen in HI (Weliachew, Sancisi, & Guélin 1978; Rand 1994), and more recently to a lesser extent in cold dust (Neininger & Dumke 1999). It also shows two large and highly energetic HI supershells (Rand & van der Hulst 1993),

the origin of which is not clear (Rand & Stone 1996; Loeb & Perna 1998). The disturbances to the disk resulting from the interactions may have caused the rather high level of star formation [ $L_{H\alpha} = 1.6 \times 10^{41}$  ergs  $s^{-1}$ , uncorrected for internal extinction (Rand, Kulkarni & Hester 1992)].

The above-mentioned gaseous halos are particularly bright above the central 4 kpc of the disk, where almost all of the  $^{12}\text{CO } J = 1 - 0$  emission is found (Golla & Wielebinski 1994; hereafter GW). The CO observations show a rigidly rotating inner disk with a total molecular mass of  $9 \times 10^8 M_{\odot}$ . Whether the inner 4-kpc structure might be a bar is a subject of debate (e.g. Roy, Wang, & Arsenault 1991; GW). It is conceivable that the interactions have driven much of the dense ISM into the central regions of the galaxy, providing the fuel for the strong star formation activity.

NGC 4631 provides us with an excellent opportunity to study star formation, galaxy interactions, possible radial inflows, and the production of gaseous halos, and thus deserves continued investigation. Therefore, to probe further the structure and kinematics of the central concentration of dense gas, we have observed it in the  $^{12}\text{CO } J = 1 - 0$  line with the Berkeley-Illinois-Maryland Array (BIMA).

## 2. Observations

The data were taken in September 1995 in the C configuration of the BIMA array, with baselines ranging from 12 to 52 m. A single track was obtained, with an approximate on-source integration time of five hours. The primary beam of the antennae is  $100''$  at the 2.6 mm wavelength of the  $^{12}\text{CO } J = 1 - 0$  transition. The quasar 3C273 was used for flux calibration. While observing NGC 4631, pointing was switched every 50 seconds between two positions with offsets of  $25''$  east and  $15''$  west of a position near the radio nucleus [R.A.  $12^{\text{h}} 42^{\text{m}} 07.7^{\text{s}}$ , Dec.  $32^{\circ} 32' 29''$  (2000.0); Duric, Seaquist, & Crane 1982), ensuring that the all of the entire bright emission from the central regions mapped by GW was contained within the primary beams. Calibration, mapping, and cleaning were carried out with the MIRIAD package (Sault et al. 1995), using the 'mosaic' option in the program 'invert' to create a mosaic dirty map of the two fields. The emission was bright enough to allow self-calibration to be performed. For each pointing a clean map was initially produced and used as a model in the MIRIAD program 'selfcal'. The self-calibrated  $uv$ -data were then used to create a new clean map, which became the new model for the next iteration. Convergence was achieved after four iterations. The clean beam has dimensions  $9.8'' \times 6.7''$  (P.A.  $-82^{\circ}$ ). The noise in the final channel maps is  $130 \text{ mJy (beam)}^{-1}$  or  $0.2 \text{ K}$ . A total intensity map was formed from emission in the range  $V_{lsr} = 440 - 820 \text{ km s}^{-1}$ , using data above  $2\sigma$  in each channel. The systemic velocity of NGC 4631 is  $V_{lsr,sys} = 618 \text{ km s}^{-1}$  (Rand 1994), and we adopt the commonly used distance of 7.5 Mpc (Hummel, Sancisi, & Ekers 1984).

### 3. Results

#### 3.1. General Structure

Figure 1 shows the map of total CO intensity, including the FWHM of the primary beam for the two pointings, while Figure 2 shows the same map overlaid on H $\alpha$  and red-continuum CCD images from Rand, Kulkarni, & Hester (1992). Some emission at the western end of the CO distribution is beyond the FWHM of the western primary beam and may not be real or accurately mapped. Other isolated features above the plane which reach only the first contour level ( $2\sigma$ ) are not significant enough to be considered real. Position-velocity diagrams parallel to the major axis of the galaxy are shown in Figure 3. The major axis position angle of  $86^\circ$  is the large-scale value derived from HI data (Rand 1994).

The basic CO structure and kinematics of the central region have been analyzed in detail by GW; hence, we only briefly discuss them here, and focus on the small-scale features revealed by the high resolution (§3.2). The emission shows a continuous structure with maxima at either end. The central minimum is at the position of the HI kinematic center (Rand 1994). The brightening towards the far ends of these features is consistent with previous single-dish observations (GW; Sofue et al. 1990; Sofue, Handa, & Nakai 1989), and suggests a ring or bar-like structure of length  $\sim 4$  kpc. The spectra of GW show that the emission falls off sharply beyond the radius of this structure. The “bend” noted by GW is even more noticeable here: the eastern half is elongated along a position angle  $\approx 90^\circ$  while the position angle of the western half is  $75 - 80^\circ$ . In this way, the central region reflects the well-known overall bend of the galaxy. This bend causes an exaggeration of the E-W asymmetry of the emission in the position-velocity ( $l - v$ ) diagrams: with the northern (southern) slices showing brighter emission from the eastern (western) end. The midplane  $l - v$  diagram indicates rigid rotation with a slope of  $1.9 \text{ km s}^{-1} \text{ arcsec}^{-1}$ , in agreement with the slope measured from the CO 2–1 map of GW. Velocities reach about  $130 \text{ km s}^{-1}$  from the systemic velocity.

The bright concentration at the eastern end of the emission shows a two-peaked velocity profile in a few cuts in Figure 3. The concentration at the western end does not show a clear bifurcation, but the velocity width is relatively large, similar to the eastern concentration. These kinematics could be due to localized events (see §3.2), or they may indicate non-circular motions. In particular, at the ends of a bar, gas streaming nearly perpendicular to the bar – on nearly circular orbits where the spiral pattern begins – may run into gas streaming along the bar (e.g. Regan, Vogel, & Teuben 1997), creating a shock (see also Roberts, Huntley, & van Albada 1979) or at least orbit crowding. The CO velocity field at the transition between the bar and the spiral arms in M83 has been interpreted in this way (Kenney & Lord 1991). This flow convergence may lead to bright regions of star formation, as observed at the ends of many bars, although more often in SBb galaxies (Phillips 1993). A high level of star formation at this CO peak is indicated by bright H $\alpha$ , X-ray and radio continuum emission, as discussed in §3.2.

Against the bar hypothesis is the fact that nothing else in the  $l - v$  diagram strongly suggests a bar, such as the expected “parallelogram” appearance of the emission due to  $x_1$  orbits parallel to the bar potential (Binney et al. 1991). This conclusion was also reached by GW. Only for a bar viewed side-on do the  $x_1$  orbits occupy a narrow locus in  $l - v$  diagrams (see Figure 8 of García-Burillo & Guélin 1995). In support of such a perspective is that NGC 4631 has one of the most slowly rising CO rotation curves of the 14 galaxies studied by Sofue et al. (1997), as might be expected for a side-on view of a bar. However, the low slope of the rotation curve could simply be due to the almost complete lack of a visible bulge. Furthermore, there is no indication of gas on  $x_2$  orbits perpendicular to the bar, deep in the potential (cf. Figure 1 of Binney et al. 1991). These are particularly noticeable in side-on views. A lack of molecular gas in the inner parts of the bar could be responsible. Alternatively, the bar may not have an ILR (e.g. Athanassoula 1992). For the modeled HI rotation curve of Rand (1994), this would imply a bar pattern speed of  $\gtrsim 20 \text{ km s}^{-1} \text{ kpc}^{-1}$ . Hence, a bar cannot be ruled out but there is little evidence to support anything more complex than a ring structure. Nevertheless, even a ring may represent a resonant response to a bar potential, but again there is little supporting evidence for a bar, particularly in the stellar emission (see below). There may still be lower-level non-circular motions, however, given that slightly non-axisymmetric bulges are common in spirals (Zaritsky & Lo 1986), and given the many other disturbances to this galaxy.

HI data in this central region show a rise in velocity very similar to the CO data, but no evidence of a central minimum. It is more difficult to discern a bar in the HI data because of confusion with the larger, differentially-rotating disk. There is evidence of broadened velocity profiles in the central  $4'$ . The model HI cube of Rand (1994) featured a velocity dispersion dictated by the rate of falloff of emission at the terminal velocity in the differentially rotating component. This choice produced generally broader profiles than observed in the central  $4'$ , most likely indicating non-circular motions, but whether they are due to an inner bar or to spiral structure cannot be determined.

The disturbed optical appearance in the central regions, the lack of a discernable bulge, and the lack of near-IR imaging of this galaxy make it difficult to appeal to the stellar distribution to aid in discerning a bar. Such a structure might be inferred from a boxy or peanut-shaped bulge, as in, for example, NGC 4013, where the CO distribution clearly shows evidence for bar-driven orbits (García-Burillo, Combes, & Neri 1999). In NGC 4631, the central regions in the red image (Figure 2b) show a very irregular morphology, due to some combination of irregular stellar and dust distributions.

The central regions of NGC 4631 have been recently mapped in submillimeter continuum emission by three different groups (Braine et al. 1995; Alton, Davies, & Bianchi 1999; Neininger & Dumke 1995). The CO map in general resembles these maps rather well in that they all show a central structure of about 4 kpc extent with emission enhancements near the ends. The prominent extraplanar feature seen in the 1.3mm continuum map of Braine et al. (1995), extending about  $1'$  southward of the eastern complex, is not seen in CO. It is not likely to have been resolved

out, since essentially all of its structure is on scales to which the CO map is sensitive. Using the conversion of 1.3mm surface brightness to gas mass given by Braine et al., the typical gas surface density in this filament should be of order  $200 M_{\odot} \text{ pc}^{-2}$ . If all of this gas were molecular and detectable in CO, we should expect emission in our map at a typical level of  $30 \text{ Jy (beam)}^{-1} \text{ km s}^{-1}$ , or  $6\sigma$ . This is clearly not seen. Possibilities are that the dust is associated with HI gas, the gas to dust ratio is much lower in NGC 4631, any molecular gas in the spur is too cold to emit substantially in the CO lines, or the emission is spurious. For the main central  $2'$  feature at least, the agreement of the derived mass with the total HI+H<sub>2</sub> mass is better than a factor of 2 (Braine et al.), suggesting that the essential conversion from 1.3mm emission to total gas mass is reasonably accurate. It is difficult to extend this conclusion to the high- $z$  gas, however. More relevant is that the feature is not seen in the 1.2mm map of Neininger & Dumke (1999), which has very similar resolution and sensitivity. It may well be spurious.

On the other hand, the beginnings of the loop south of the nucleus in Braine et al.'s map coincide with a CO spur extending south from the western half of the emission; these in turn may be associated with an extraplanar H $\alpha$  feature (Figure 2). The  $850 \mu\text{m}$  continuum map of Alton et al. (1999) also shows extraplanar emission just south of this CO spur.

The 1.4 GHz map of Golla (1999) at  $1.45''$  resolution shows much agreement with the CO distribution on scales of a few arcseconds, including bright concentrations coincident with the two CO peaks at each end of the main structure, and a relative deficit of emission between them. Earlier radio maps also show a concentration of synchrotron emission in the central 4 kpc of the disk (e.g. Ekers & Sancisi 1977, Duric et al. 1982; Golla & Hummel 1994).

Most of the diffuse extraplanar H $\alpha$  emission (Figure 2; see also Hoopes, Walterbos, & Rand 1999) is found above and below the 4-kpc extent of the CO emission. The quasi-vertical double-worm structure reported by RKH does not rise from the center of the CO structure but from a position about 700 pc to the east. Diffuse, soft X-ray halo emission generally surrounds the inner disk and is brightest in the approximate radial range of the CO emission, as seen in the overlay of the ROSAT PSPC map from Vogler & Pietsch (1996), kindly provided by A. Vogler, and the CO map in Figure 4a (see also Wang et al. 1995). Finally, bright polarized emission at 4.88 and 8.46 GHz is found in the halo above this region of the disk, where the inferred intrinsic magnetic field runs largely perpendicular to the major axis (Golla & Hummel 1994). All of these associations suggest active star formation and outflow of gas into the halo. All three halo tracers are brighter on the north side of the CO emission than the south side.

Assuming a conversion between CO brightness and H<sub>2</sub> column density of  $X = 2.3 \times 10^{20} \text{ mol cm}^{-2} (\text{K km s}^{-1})^{-1}$ , the total molecular mass detected is  $1.0 \times 10^9 M_{\odot}$ . Within the uncertainties, this value agrees with the estimate of GW for the central  $140''$  (using the same value of  $X$ ), suggesting that little, if any, emission has been resolved out by our observations.

### 3.2. An Unusual Extraplanar Feature

The most important new result from this observation is the filamentary and shell-like emission found north of the eastern end of the main CO feature. A weaker feature is also seen to the south. The extraplanar emission is detected up to 750 pc above the midplane of the CO distribution. Although the galaxy is not quite edge-on, it is unlikely that the feature is in the plane of the galaxy. At  $i = 86^\circ$ , it would have to extend about 10 kpc along the midplane to explain the apparent extent parallel to the minor axis. Also, kinematically, in a highly inclined, differentially rotating disk, one would expect the feature to show a smooth gradient towards lower observed velocities with increasing distance from the major axis if it were in the disk. Although its kinematics are complex (see below), it does not show such a signature. The mass of the feature is estimated at roughly  $10^8 M_\odot$ , using the above value of  $X$ . It splits into a quasi-linear feature on the west side, rising to the north-west, and a more shell-like feature on the east side, suggesting that it may have been produced by two events.

Figure 5 shows position-velocity diagrams parallel to the R.A. axis in the region of this feature, covering its full vertical extent. The disk emission below the feature is the brightest in the map and kinematically splits into two components, as discussed above, with the lower velocity component deviating somewhat from the general trend of velocity with position. Just to the east of the bright disk feature, most of the emission centers around  $V_{lsr} \approx 750 \text{ km s}^{-1}$ , while fainter emission is seen at  $V_{lsr} \approx 680 \text{ km s}^{-1}$  (more apparent in the  $-3''$  panel).

Velocities in the western, filamentary component of the extraplanar feature (best seen in the 12, 15 and 18'' panels at R.A. offsets around  $-12''$ ) center around  $V_{lsr} = 680 \text{ km s}^{-1}$ , a typical velocity for its distance along the major axis, and no clear trend of velocity with position can be identified as a clue to its nature. However, in the eastern extraplanar feature (around R.A. offset  $12''$ ), the two disk components at  $V_{lsr} \approx 750 \text{ km s}^{-1}$  and  $V_{lsr} \approx 680 \text{ km s}^{-1}$  are seen up to the 15'' panel (also to the  $-6''$  panel). This velocity splitting may indicate a structure expanding at  $v \approx 70 \text{ km s}^{-1}$ . Given that the eastern feature accounts for slightly more than half the emission, the equivalent kinetic energy of a spherically expanding shell would be enormous:  $2 - 3 \times 10^{54}$  erg, comparable to the two HI supershells. On the other hand, there are other possible sources of peculiar kinematics at this radius, as discussed above, and the line splitting may have an orbital origin, although the evidence is inconclusive.

Another indication of the energy involved in creating such an outflow comes from an estimate of the potential energy of the gas mass at its height above the plane. This has been estimated for several dust clouds above the disk of NGC 891 by Howk & Savage (1997). Unfortunately, the estimate depends on the rather poorly known total midplane mass density and scale height. The potential energy is given by:

$$\Omega = 10^{52} \text{ ergs} \left( \frac{M}{10^5 M_\odot} \right) \left( \frac{z_0}{700 \text{ pc}} \right) \left( \frac{\rho_0}{0.185 M_\odot \text{ pc}^{-3}} \right) \ln[\cosh(z/z_0)] \quad (1)$$

where  $z_0$  is the total mass scale height,  $\rho_0$  is the total midplane mass density and  $M$  is the mass of

the high- $z$  feature. The  $B$ -band scale-height has been determined by Hummel & Dettmar (1990) to be about 1 kpc. This may be a poor estimate of the true mass scale height, which itself could vary significantly around this disturbed galaxy. However, use of this value should still give a rough estimate of the energies involved. The total mass density is unknown but presumably less than in NGC 891 or the Milky Way given the low rotation speed of  $140 \text{ km s}^{-1}$  (Rand 1994). Using the above molecular gas mass and an average height above the plane of 500 pc, the potential energy is then

$$\Omega = 2 \times 10^{54} \text{ ergs} \left( \frac{\rho_0}{0.185 M_{\odot} \text{pc}^{-3}} \right) \quad (2)$$

comparable to the kinetic energy estimate. Of course, this analysis does not account for energy radiated away or converted to thermal or turbulent motions.

The bright disk emission below this feature abuts the western edge of the very bright complex of HII regions CM65, CM66, and CM67 (Crillon & Monnet 1969; Roy et al. 1991), suggesting a region of intense star formation. In fact, the eastern, shell-like extraplanar feature almost appears to surround the peak of  $\text{H}\alpha$  (and associated red continuum) emission (Figure 2). The  $\text{H}\alpha$  luminosity from this complex, measured from the image of Rand, Kulkarni, & Hester (1992), is  $6 \times 10^{39} \text{ erg s}^{-1}$  (uncorrected for extinction), about equal to that of 30 Doradus in the LMC (Kennicutt & Hodge 1986). Roy et al. (1991) noted a complex velocity structure for these HII regions, with components at  $V_{lsr} = 641, 687, \text{ and } 753 \text{ km s}^{-1}$ . Thus, both CO and  $\text{H}\alpha$  emission show a large range of velocities, and there is some correlation of these components between the two tracers. Of course, it must be recalled that the disk emission may have a significant extent along the line of sight (for instance if it is part of a ring viewed along the tangent point), and this may explain, at least in part, why it is so bright in several ISM tracers. There are no well-defined *extraplanar*  $\text{H}\alpha$  features which are associated with the CO emission. In particular, the double-worm structure lies between this CO structure and the center of the molecular ring. It may originate from a star-forming complex elsewhere on the ring.

X-rays from this part of the disk provide further evidence for a high rate of star formation. Figure 4b shows the CO emission with contours of X-ray emission from the “adaptive-filtered” ROSAT HRI (0.1–2.4 keV) image of Vogler & Pietsch (1996). The filtering technique smooths the original HRI image with a kernel whose size depends on the image intensity, thus enhancing low-level diffuse emission while retaining high resolution for bright, compact features. No X-ray feature can be specifically associated with the molecular outflow, but the bright concentration of disk CO emission beneath it is coincident within the positional uncertainties with the brightest peak of X-ray emission in the inner disk. This source has a luminosity, corrected for Galactic absorption, of  $8 \pm 3 \times 10^{37} \text{ erg s}^{-1}$  (0.1–2.4 keV), and is too weak to obtain a spectrum. This luminosity is a lower limit due to unaccounted for absorption in NGC 4631, and is comparable to those of the X-ray sources in M101 postulated to be supernova remnants by Wang (1999).

Coincident with these disk CO and X-ray sources is a bright source of radio emission in Golla’s (1999) 1.4 GHz map at 1.45”. This source resolves into five features in a 4.86 GHz map at

sub-arcsecond resolution, four of which have thermal spectra. Golla & Hummel (1994) trace one of the radio continuum spurs back down to the CM67 region in the disk. None of the extraplanar emission from cold dust found by Neininger & Dumke (1999) appears to be associated with the CO feature. Examination of the HI data cube of NGC 4631 at 12"x22" (Rand 1994) shows no obvious associated kinematic or morphological peculiarities.

Hence, there is much evidence for a very intense region of star formation at in this disk location, and an extraplanar radio continuum filament also seems to be associated with the CO feature.

### 3.3. Possible Origins of the Extraplanar Feature

It is difficult to conclude much about the origin of this feature at this point. If the kinetic energy is of order  $10^{54}$  ergs, then it may be difficult to explain it as a result of stellar winds and supernovae, as was the case for the two large HI supershells (Rand & van der Hulst 1993). One would require of order 10,000 supernova progenitors. Alternatively, it may be due to the impact of a rather massive high-velocity cloud, an explanation considered by Rand & Stone (1996) for the HI supershells (there, an impactor of about  $10^7 M_{\odot}$  was required). The impact may have triggered the star formation in the disk at this location. In this case, the X-ray emission would be due to the resulting supernovae, as the collision itself would not be able to heat gas to X-ray emitting temperatures. An examination of the HI data of Rand (1994) does not reveal any obvious signs of an impact at this location, such as a trail of gas. Finally, there is the newly recognized possibility that such shells can be produced by a single energetic explosion – a hypernova, which may be the cause of gamma-ray bursts (e.g. Loeb & Perna 1998; Efremov, Elmegreen, & Hodge 1998; Wang 1999). At best, it is difficult to distinguish between putative hypernovae and conventional supernova-driven supershells, and in this case especially so, given the difficulty of disentangling emission along the line of sight, correcting X-ray fluxes for absorption in the intervening gas, and determining the age of the high- $z$  structure. However, it is worth noting that this is now the third problematically energetic event found in this galaxy. This may provide constraints on the hypernova hypothesis. Whether these events occur because of hypernovae, or multiple supernovae and stellar winds from massive star formation concentrated into unusually large associations, or a few relatively massive high-velocity clouds penetrating the disk, can only be answered by future investigation. The CO emission from the feature reported here is bright enough to allow a higher resolution map to be made. Such a map may provide a clearer delineation of its morphology and kinematics, allowing a more careful comparison with models of its origin. Also Chandra, with its higher resolution compared to ROSAT, may constrain the nature of the X-ray emission by showing whether it remains diffuse on smaller scales or breaks up into multiple components, and also by allowing a measurement of the gas temperature.



#### 4. Conclusions

In this brief paper we have presented a high-resolution map of the centrally concentrated CO emission in NGC 4631. The map confirms the ring or bar-like distribution of molecular gas inferred from single-dish data, but there is little direct evidence for a bar. Halo emission in several gaseous tracers is concentrated above, and to a lesser extent, below, this molecular structure, suggesting that the central concentration of molecular gas has provided the fuel for intense star formation which has resulted in a substantial outflow of gas.

Of great interest is an extraplanar CO feature found above the eastern end of the molecular structure. It suggests an outflow of about  $10^8 M_{\odot}$  of molecular gas, although there is only weak evidence for an associated kinematic signature. Nevertheless, the energies involved in driving the outflow may be well over  $10^{54}$  ergs. Bright HII regions and X-ray emission suggest that the underlying disk location is very active in star formation. An extraplanar radio continuum filament also appears to have a footprint in this region. Like the two highly energetic HI supershells in this galaxy, this outflow may be driven by multiple supernovae or is perhaps the result of an impact of a high-velocity cloud. Its characteristics also put it in the class of events postulated to be due to hypernova explosions.

This research has made use of the NASA/IPAC Extragalactic Database (NED) which is operated by the Jet Propulsion Laboratory, California Institute of Technology, under contract with the National Aeronautics and Space Administration.

We are grateful to W. Pietsch and A. Vogler for providing the ROSAT images, and to P. Teuben for comments on the manuscript.

#### REFERENCES

- Alton, P. B., Davies, J. I., & Bianchi, S. 1999, *A&A*, 343, 51  
Athanassoula, E. 1992, *MNRAS*, 259, 328  
Binney, J., Gerhard, O. E., Stark, A., Bally, J., & Uchida, K. I. 1991, *MNRAS*, 252, 210  
Braine, J. Krüegel, E., Sievers, A., & Wielebinski, R. 1995, *A&A*, 295, 55  
Crillon, R., & Monnet, G. 1969, *A&A*, 2, 1  
Duric, N., Seaquist, E. R. & Crane P. C. 1982, *AJ*, 87, 1671  
Efremov, Y. N., Elmegreen, B. G., & Hodge, P. W. 1998, *ApJ*, 501, 163  
Ekers, R. D., & Sancisi, R. 1977, *A&A*, 54, 973

---

<sup>0</sup>The National Radio Astronomy Observatory is operated by the Associated Universities, Inc. under cooperative agreement with the National Science Foundation.

- García-Burillo, S., Combes, F., & Neri, R. 1999, *A&A*, 343, 740
- García-Burillo, S., & Guélin, M. 1995, *A&A*, 657, 299
- Golla, G. 1999 *A&A*, 345, 778
- Golla, G. & Hummel, E. 1994 *A&A*, 284, 777
- Golla, G. & Wielebinski, R. 1994 *A&A*, 286, 733 (GW)
- Hoopes, C. G., Walterbos, R. A. M., & Rand, R.J. 1999, *ApJ*, in press
- Howk, J. C., & Savage, B. D. 1997, *AJ*, 114, 2463
- Hummel, E., & Dettmar, R.-J. 1990, *A&A*, 236, 33
- Hummel, E., Sancisi, R., & Ekers, R. D. 1984, *A&A*, 133, 1
- Kenney, J. D. P., & Lord, S. D. 1991, *ApJ*, 381, 118
- Kennicutt, R. C., & Hodge, P. W. 1986, *ApJ*, 306, 130
- Loeb, A., & Perna, R. 1998, *ApJ*, 503, 35
- Neininger, N., & Dumke, M., 1999, *PNAS*, in press
- Phillips, A. C. 1993, PhD. Thesis, Univ. of Washington
- Rand, R. J. 1994, *A&A*, 285, 833
- Rand, R. J. & van der Hulst, J. M. 1993, *AJ*, 105, 2098
- Rand, R. J., Kulkarni, S. R., & Hester, J. J., 1992, *ApJ*, 396, 97
- Rand, R. J. & Stone, J. M. 1996, *AJ*, 111, 190
- Regan, M. W., Vogel, S. N., & Teuben, P. J. 1997, *ApJ*, 482, 143
- Roberts, W. W., Huntley, J. M., & van Albada, G. D. 1979, *ApJ*, 233, 67
- Roy, J.-R., Wang, J., & Arsenault, R. 1991, *AJ*, 101, 825
- Sault, R. J., Teuben, P. J., & Wright, M. C. H. 1995, in *Astronomical Data Analysis Software and Systems IV*, ed. R. A. Shaw, H. E. Payne, & J. J. E. Hayes, ASP Conf. Series 77, 443
- Sofue, Y., Handa, T., & Nakai, N. 1989, *PASJ*, 41, 937
- Sofue, Y., Handa, T., Golla, G., & Wielebinski, R. 1990, *PASJ*, 42, 745
- Sofue, Y., Tutui, Y., Honma, M., & Tomita, A. 1997, *AJ*, 114, 2428
- Vogler, A., & Pietsch, W. 1996, *A&A*, 311, 35
- Wang, Q. D. 1999, *ApJ*, 510, 139
- Wang, Q. D., Walterbos, R. A. M., Steakley, M. F., Norman, C. A., & Braun, R. 1995, *ApJ*, 439, 176
- Weliachew, L., Sancisi, R., & Guélin, M. 1978, *A&A*, 65, 37

Zaritsky, D., & Lo, K. Y. 1986, ApJ, 303, 66

---

This preprint was prepared with the AAS L<sup>A</sup>T<sub>E</sub>X macros v4.0.

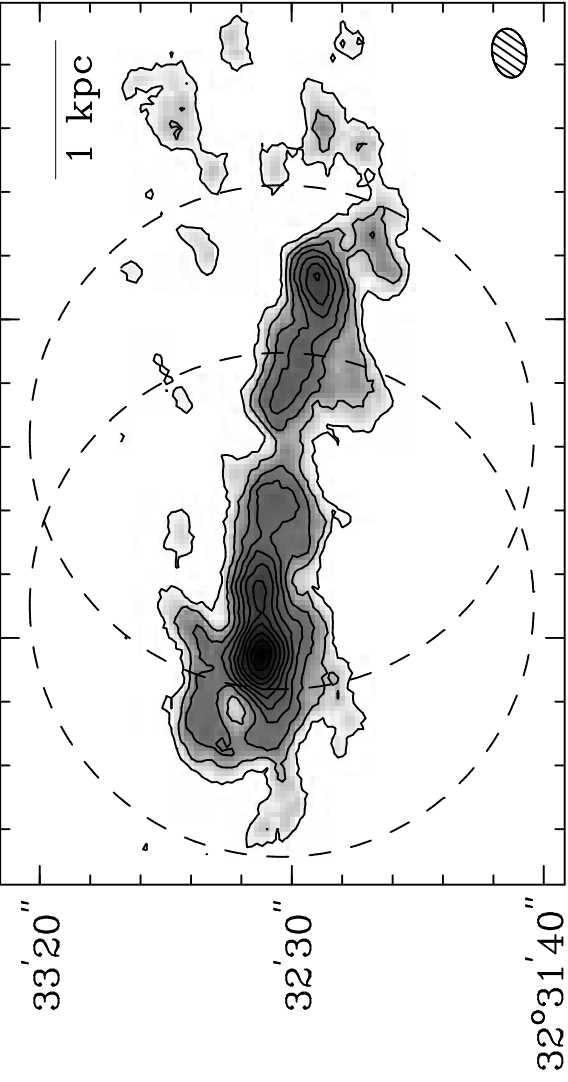
Fig. 1.— Map of total CO intensity at  $9.8 \times 6.7''$  resolution. The dashed circles indicate the HPBW of the primary beam for the two pointings. The clean beam is shown at lower right. A bar corresponding to a length of 1 kpc is also shown. Contour levels are 10 to 180 Jy (beam)<sup>-1</sup> km s<sup>-1</sup> in steps of 15 Jy (beam)<sup>-1</sup> km s<sup>-1</sup>. The  $1\sigma$  noise in this map is about 5 Jy (beam)<sup>-1</sup>.

Fig. 2.— Contours of CO emission overlaid on *a*) an H $\alpha$  image of NGC 4631 showing the central  $\sim 13$  kpc of the disk, and *b*) a red image showing the central  $\sim 7$  kpc of the disk (both from Rand, Kulkarni, & Hester 1992). Both optical images are displayed on a logarithmic scale. Contour levels are as in Figure 1. Spillover due to a bright star is present in both optical images.

Fig. 3.— Major axis position-velocity diagrams along a position angle of  $86^\circ$ . East is to the left. Slices are spaced by  $3''$  perpendicular to the major axis. The central slice has its origin at R.A.  $12^{\text{h}} 42^{\text{m}}07.7^{\text{s}}$ , Dec.  $32^\circ 32' 29''$ . Contour levels are  $-0.3$  to  $2.7$  Jy (beam) $^{-1}$  in steps of  $0.3$  Jy (beam) $^{-1}$  (about  $2.3\sigma$ ).

Fig. 4.— Contours of CO emission overlaid on the central part of the (a) ROSAT PSPC image and (b) ROSAT HRI image from Vogler & Pietsch (1996). Contour levels are as in Figure 1.

Fig. 5.— Position-velocity diagrams along a position angle of  $90^\circ$  for the eastern end of the main emission. Slices are spaced by  $3''$  perpendicular to the major axis. The central slice has its origin at R.A.  $12^{\text{h}} 42^{\text{m}}10.47^{\text{s}}$ , Dec.  $32^\circ 32' 35''$ . Contour levels are as in Figure 3.



12<sup>h</sup>42<sup>m</sup>10<sup>s</sup> 5<sup>s</sup>  
Right Ascension (2000.0)

